10th ANKARA INTERNATIONAL AEROSPACE CONFERENCE **AIAC-2019-119**
18-20 September 2019 - METU, Ankara TURKEY

PERFORMANCE COMPARISON OF SU2 REAL GAS MODELS AND TESTING FOR A COLD GAS THRUSTER

Aysu Özden[1], Ö. Uğraş Baran[2] M. Haluk Aksel[3]
Middle East Technical University
Ankara, Turkey

Mehmet Ali Ak[4]
ROKETSAN A.Ş.
Ankara, Turkey

ABSTRACT

Cold gas propulsion systems are mainly used for attitude control of satellites. It is possible to obtain very low pressure and temperature at the exit section of the nozzle due to propulsion system's nature. Investigation of steady state performance of a cold gas thruster under real gas effects is decided to be carried out. SU^2, an open source compressible CFD tool, is used for analyses of ideal gas, Peng-Robinson and van-der Waals gas models. Vacuum chamber test facility of Roketsan is used for performance tests. Results showed that van der Waals gas model in SU^2 is good enough for predictions of cold gas thruster's performance.

INTRODUCTION

Cold gas propulsion systems have been used in small satellites since 1960's. These systems are mostly chosen due to their cost effectiveness, lower mass, design simplicity and compatibility. Their simple construction provides high reliability. However, their low thrust and low specific impulse values make these systems to remain behind the chemical propulsion systems. Achievable thrust is only up to 10 N and available propellant is limited by the propellant's physical state and volume of the tank [Zandbergen, 2000].

Cold gas propulsion systems usually consist of a propellant tank, pipeline to deliver propellant to the rest of the system, valves to control the propellant supplied to the thruster and thrusters themselves. Schematic drawing of a sample cold gas propulsion system with its components is given in Figure 1.

[1] MSc. Student in Mechanical Engineering Department, Email: e194074@metu.edu.tr
[2] Assist. Prof. Dr. in Mechanical Engineering Department, Email: ubaran@metu.edu.tr
[3] Prof. in Mechanical Engineering Department, Email: aksel@metu.edu.tr
[4] Manager, Email: mehmetaliak@roketsan.com.tr

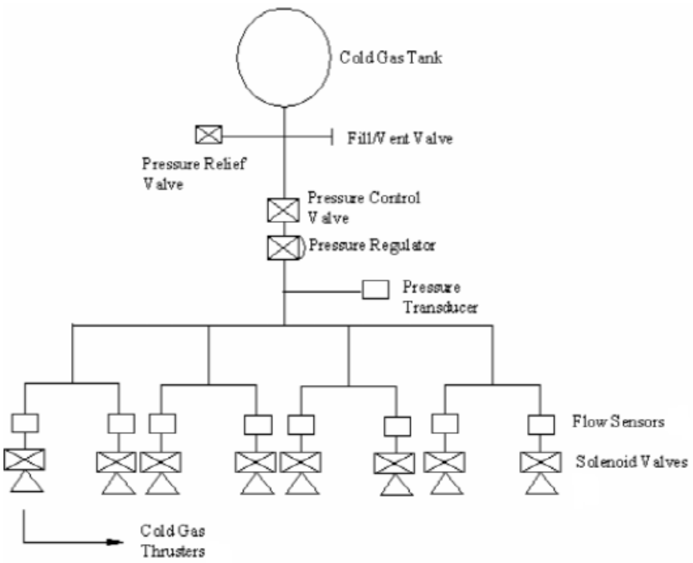

Figure 1: Schematic drawing of a cold gas propulsion system with main components [Anis, 2012]

Thrust is obtained by expelling high pressure gas through the nozzle using only available enthalpy of the propellant without any combustion, heat addition or any other mechanisms to add energy [Lemmer, 2017]. There are three different cold gas propulsion systems according to their working principles; pressurized gas systems, heated gas systems and liquefied gas systems. General schematics of these systems are shown in Figure 2 . Pressurized gas system is taken into account for the present study.

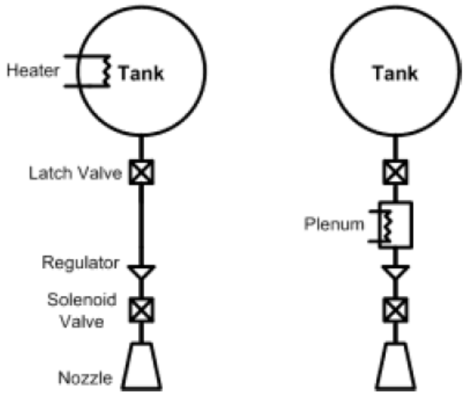

Figure 2: Cold gas propulsion systems from left to right; pressurized gas system, heated gas system and liquefied gas system [Lev, Herscovitz, and Zuckerman, 2014]

Pressurized gas systems are the simplest ones with respect to its working principle. A tank which is used to store high pressurized propellant, followed by latch valve, which protects the rest of the system from high pressurized propellant prior to operation. Following the actuation of the latch valve, high pressure gas is lowered to operational pressure by a pressure regulator. Finally, a solenoid valve is actuated to supply the propellant to the thrust chamber. Relatively high pressured gas is expanded and accelerated through a nozzle in order to obtain thrust.

There are several cold gas propulsion systems, which are successfully operated in space. One of them is CanX-2, which was launched in April 2008 with Nano Propulsion System (NANOPS) with thrusters using sulfur hexafluoride [Sarda, Grant, Eagleson, Kekez, and Zee, 2008]. Another propulsion system, which was integrated to CanX-5 satellite, was the Canadian

Nanosatellite Advanced Propulsion System (CNAPS) having thrusters which was using sulfur hexafluoride as the propellant [Risi, 2014]. The Aerospace Corporation manufactured another propulsion system for the Microelectromechanical System PICOSAT Inspector in 2006. Thrusters of this system are using Xenon as the propellant [Hinkley, 2008]. Argon is utilized in the thrusters of Propulsion Operation Proof SATellite - High Performance 1 (POP AT-HIP1) which was fired in 2014 [Manzoni, and Brama, 2015].

There are many criteria for choosing the propellant used in the system. Having a contamination-free propellant is useful since expelled propellant would not have residues which may interfere with sensing devices or mechanical actuators [Bzibziak, 2000]. Also, in terms of handling and storage, moderately low boiling point and melting temperature and mass efficient propellants are considered [Jerman, and Langus, 2011]. Among gaseous propellants, nitrogen, oxygen, hydrogen, helium, argon and xenon are the most preferred ones. Nitrogen is the mostly chosen propellant among other alternatives due to its storage density, performance and lack of contamination aspects.

Thrusters are one of the most critical components of a cold gas propulsion system for delivering the desired performance. Thruster is a combination of a thrust chamber, which contains the required volume for the propellant and a nozzle to accelerate the propellant and obtain thrust. Nozzles used in these systems can be converging or converging-diverging (de Laval). Since it is possible to obtain higher performance with converging-diverging nozzles, they are frequently studied in the literature. De Laval nozzle is designed such that flow through its throat reaches sonic velocity in order to obtain maximum allowable mass flow rate and the desired maximum allowable thrust. Diverging section of a nozzle can be conical or bell type, as shown in Figure 3. The geometric dimensions of the throat of a cold gas thruster are quite small for obtaining the required performance. Also, since these thrusters are used in space, they are designed to expand to vacuum. Expansion to vacuum results in longer diverging sections. Considering ease of manufacturing and design procedure, conical nozzles are preferred for practical applications.

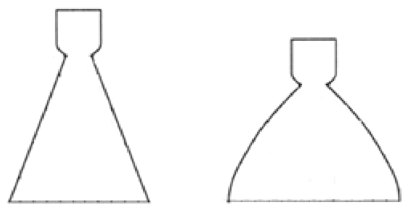

Figure 3: Conical nozzle (left) and bell type nozzle (right)

Design procedure of a conical nozzle requires to define a loss coefficient for losses due to its divergent geometry and flow conditions. Loss coefficient can be calculated by using the following equation [Shephered, 1972]:

$$\lambda = (1 + \cos\alpha)/2 \qquad \text{E. 1}$$

Half cone angle (α) is another design parameter. Ahmer et. al. (2014) studied the effect of three different angles, 8°, 15° and 25°. Under same conditions, it was observed that there exists slight difference in velocity between these models. It was observed that velocity was decreasing with the increasing half cone angle. However, increase in the half cone angle results in a longer nozzle. Hence, 15° was chosen as the optimum divergence angle when velocity and nozzle length are considered.

Studies in the Literature

There exists a number of numerical and experimental studies in the literature for evaluating the performance of a cold gas thruster. Matticari et. al. [Matticari, Noci, Siciliano, Miccolis, and Strada, 2010] studied a cold gas propulsion system both numerically and experimentally. Xenon was the propellant used and numerical simulations were performed for 2D axisymmetric flow domain with a commercial CFD tool by considering viscous effects [Matticari, Noci, Siciliano, Miccolis, and Strada, 2010]. Pressure, velocity and temperature were investigated. Pressure and temperature contours are provided in Figure 4.

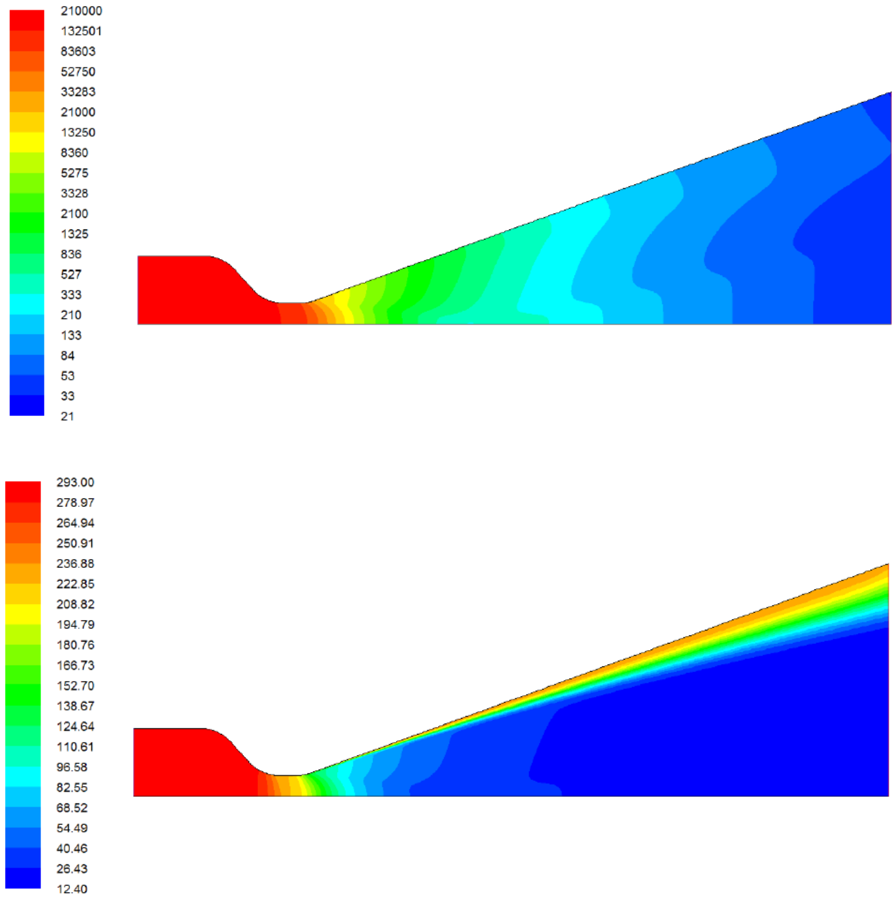

Figure 4: Pressure and temperature contours of numerical results of Matticari et. al.'s study [Matticari, Noci, Siciliano, Miccolis, and Strada, 2010]

The nozzle has an exit gas temperature of 12.40 K for an exit pressure of 21 Pa. These low temperature and pressure values give rise to a question of possibility of phase change of the propellant at some section of the thruster nozzle. Experimental study was conducted in the vacuum chamber facility at ESTEC Electronic Propulsion Laboratory [Matticari, Noci, Siciliano, Miccolis, and Strada, 2010]. Mass flow rate, gas inlet temperature and pressure were tracked during the performance tests. In case of a phase change, it was expected to have lower thrust than expected. However, experimental results did not show any performance loss. Similar study was found in the literature by Ranjan et.al. [Ranjan, Chou, Riaz, and Karthikeyan, 2017]. A cold gas thruster, which used compressed air as the propellant, was investigated. Numerical simulations showed that the exit temperature of the nozzle was approximately 35 K for vacuum operation conditions [Ranjan, Chou, Riaz, and Karthikeyan, 2017]. Yet, experiments conducted in vacuum chamber showed that predictions of numerical studies and results of experiments for thrust and specific impulse were in a good agreement.

Some studies in the literature also investigated how SU^2 is capable to solve problems including real gas as the working fluid. In ORC (Organic Rankine Cycle) applications, it is stated that when temperature and pressure of the gas are close to the critical point of the propellant, behavior of the propellant diverges from ideal gas behavior. Numerical simulation of ideal gas, van der Waals gas and Peng-Robinson Stryjek-Vera models were performed by using SU^2 and these results were compared with the outputs of integral balance equations [Gori, Guardone, Vitale, Head, Pini and Colonna, 2015]. This comparison showed that, SU^2 had the capability of dealing with non-ideal compressible flows. Pini et. al. [Pini, Vitale,Colonna, Gori, Guardone, Economon, Alonso and Palacios, 2017] studied the flow in a nozzle to show whether SU^2 was capable of solving real gas equations for nozzle applications. 2^{nd} order Roe scheme was used for space discretization. Navier-Stokes equations using implicit Euler algorithm based on CFL adaptation were solved [Pini, Vitale,Colonna, Gori, Guardone, Economon, Alonso and Palacios, 2017]. SU^2 results for Span-Wagner equation of state were compared with ANSYS-CFX results for verification. It was observed that results were matching fairly well. Mach contours and pressure ratio comparison are provided in Figure 5. It was concluded that SU2 was capable of solving non-ideal compressible flow regime problems.

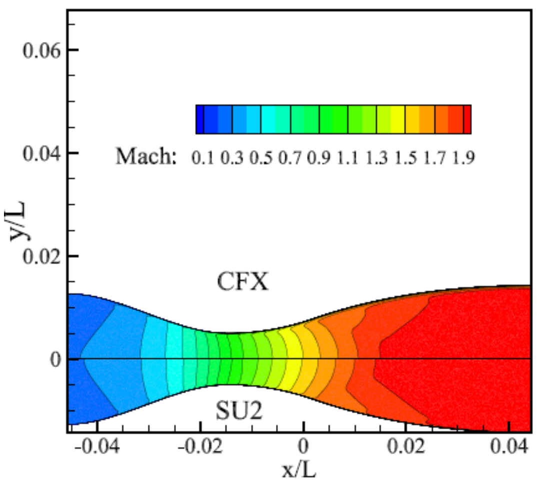

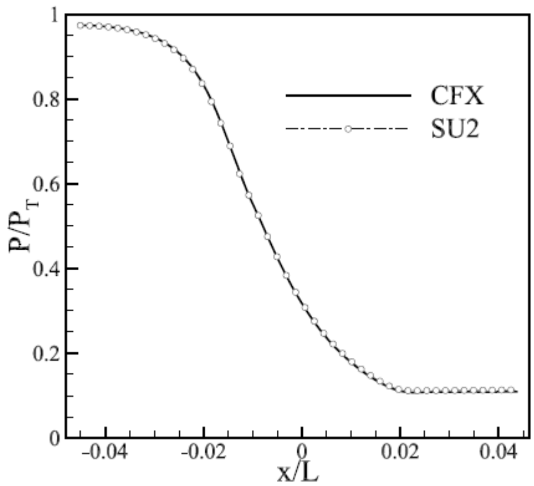

Figure 5: Mach contour (left) and centerline pressure ratio (right) comparison of SU2 with CFX [Pini, Vitale,Colonna, Gori, Guardone, Economon, Alonso and Palacios, 2017]

Design and testing of Pakistan's first cold gas propulsion system's prototype was studied by Anis [Anis, 2012]. This system was using eight 1 N thrusters which were operating at 8 bar chamber pressure. Compressed nitrogen was chosen as the propellant. Thrusters used in this prototype were conical nozzles with 16° half angle, area ratio of 50:1 and nozzle efficiency was taken as 98% [Anis, 2012], [Anis, 2008]. A test bench using a load cell was used as shown in Figure 6. As a result of thruster performance tests, it was seen that 73 s of specific impulse was obtained for continuous operation which was close to the expected value.

Figure 6: PRSS thruster (left) and static test bench (right) [Anis, 2008]

Rickmers studied experimental performance enhancement of a cold gas thruster in 2004 [Rickmers, 2004]. First the vacuum chamber in University of Bremen's Hochschule Hyperschall Kanal was used. This chamber has 1.5 m^3 volume and it can provide minimum pressure level of 10^{-3}mbar [Rickmers, 2004]. Schlieren optics, pressure and temperature sensors were used to track flow through the nozzle. Experimental study result of one of the performance tests is provided in Figure 7 in terms of pressure and thrust.

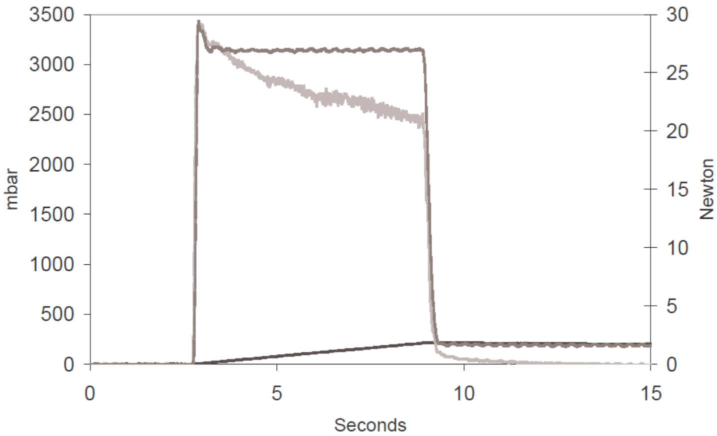

Figure 7: Time dependent pressure and thrust data of the nozzle; black line – vacuum chamber pressure, dark grey line – thrust chamber pressure and light grey line – thrust [Rickmers, 2004]

As can be seen from this figure, pressure inside the vacuum chamber increases as a result of thruster operation. Also, it is shown that both pressure and thrust responses are similar to the activation and de-activation of thruster valve. For longer tests, another facility, ZARM, was used. This facility has vacuum pumps which help to prevent pressure built up in the vacuum chamber. Throughout the tests, it was seen that the exit velocity and corresponding desired thrust were lower than theoretical values. It was concluded that the first reason was having larger ambient pressure at the nozzle exit than the theoretical calculations. Also, it was considered that boundary layer effects at the throat may decrease the mass flow rate which corresponds to lower thrust values.

METHOD

Flow field analysis of the designed thruster is carried out by using open source software since they allow more flexibility compared to commercial software. Flow simulations are aimed to be accomplished by using SU^2 by considering previous experiences of the Middle East Technical University Mechanical Engineering CFD group led by Prof. Aksel. Mesh generation is started with using Salome, whose output is not compatible with SU^2 mesh format. Gmsh and enGrid are used to define boundary conditions and obtain native SU^2 mesh format. Software used are presented in the flow diagram shown in Figure 8.

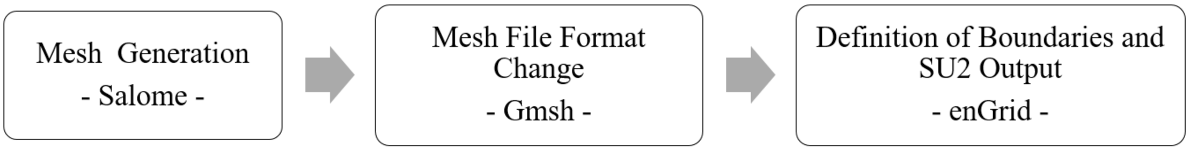

Figure 8: Tools used for mesh generation

SU[2] is capable of solving multi-physics Partial Differential Equation (PDE) problems and PDE constrained optimization problems on unstructured meshes. It is a Reynolds-Averaged Navier-Stokes (RANS) solver using on density based solvers. It allows simulations of compressible, turbulent flows.

Compressible Gas Models

As a result of applications involving non-ideal compressible flows, a built-in thermodynamic library is coupled with SU[2]. Ideal gas, van der Waals and Peng-Robinson gas models are the thermodynamic models embedded and their capabilities are investigated.

<u>Perfect Gas Thermophysical Model:</u> Perfect gas thermodynamic model is described by the following set of equations which describes polytropic ideal gas' volumetric and caloric behavior.

$$\begin{cases} p(T,v) = \dfrac{RT}{v} \\ e(T,v) = e(T) = e_{ref} + c_v(T - T_{ref}) \\ s(T,v) = s_{ref} + c_v \ln \dfrac{T}{T_{ref}} + R \ln \dfrac{v}{v_{ref}} \\ c_v = \dfrac{1}{\gamma - 1} R \end{cases} \tag{E. 2}$$

where p is the pressure, T is the temperature, R gas constant, v is the specific volume, e is the total energy per unit mass and s is the total entropy per unit mass. γ is the ratio of specific heats and can be expressed as $\gamma = \frac{c_p}{c_v}$ where c_p is the heat capacity at constant pressure and c_v is heat capacity at constant volume. These set of equations are calculated based on reference energy and entropy. Reference energy and entropy are defined as follows:

$$\begin{cases} e_{ref} = c_v T_{ref} \\ s_{ref} = -c_v \ln T_{ref} + R \ln v_{ref} \end{cases} \tag{E. 3}$$

Reference temperature and specific volume values are defined by the user at the reference pressure. These user defined values are used to non-dimensionalize the problem. As a result of this non-dimensionalization, entropy and energy equations become:

$$\begin{cases} e(T,v) = c_v T \\ s(T,v) = c_v \ln T + R \ln v \end{cases} \tag{E. 4}$$

In order to compute numerical schemes, it is necessary to calculate the thermodynamic derivatives. These derivatives are calculated for perfect gas thermodynamic equation of state as follows:

$$\left(\frac{\partial p}{\partial e}\right)_\rho = (\gamma - 1)\rho \qquad \text{E. 5}$$

$$\left(\frac{\partial p}{\partial \rho}\right)_e = (\gamma - 1)e \qquad \text{E. 6}$$

$$\left(\frac{\partial T}{\partial e}\right)_\rho = \frac{(\gamma - 1)}{R} \qquad \text{E.7}$$

$$\left(\frac{\partial T}{\partial \rho}\right)_e = 0 \qquad \text{E.8}$$

As a result of these computations, speed of sound is implemented as a function of first two properties.

$$c^2 = \left(\frac{\partial p}{\partial \rho}\right)_e + \frac{p}{\rho^2}\left(\frac{\partial p}{\partial e}\right)_\rho \qquad \text{E.9}$$

<u>van der Waals Gas Thermophysical Model:</u> The set of equations for van der Waals thermodynamic model is provided as follows:

$$\begin{cases} p(T,v) = \dfrac{RT}{v-b} - \dfrac{a}{v^2} \\ e(T,v) = c_v T - \dfrac{a}{v} \\ s(T,v) = c_v \ln T + R \ln(v-b) \end{cases} \qquad \text{E. 10}$$

This equation of state is also similar to perfect gas model in terms of its form. However, it has coefficients that change with the chemical composition and properties of the gas. The coefficient a is the measure of the intensity of the intermolecular attraction force and b is the co-volume representing the volume of the atoms or molecules in one mole of the gas.

$$\begin{cases} a = \dfrac{27}{64}\dfrac{R^2 T_{cr}^2}{p_{cr}} \\ b = \dfrac{1}{8}\dfrac{R T_{cr}}{p_{cr}} \end{cases} \quad \text{E. 11}$$

In order to calculate a and b, critical temperature and pressure of the propellant should be known. In order to conserve consistency of the equations for energy and entropy, model uses the same e_{ref} and s_{ref} defined in the perfect gas model.

Thermodynamic derivatives are also written in terms of van der Waals constants. These derivatives are provided as follows:

$$\left(\frac{\partial p}{\partial e}\right)_\rho = \frac{(\gamma - 1)\rho}{1 - \rho b} \quad \text{E. 12}$$

$$\left(\frac{\partial p}{\partial \rho}\right)_e = \frac{(e + 2\rho a - \rho^2 ab)}{\rho(1 - \rho b)}\left(\frac{\partial p}{\partial e}\right)_\rho - 2\rho a \quad \text{E. 13}$$

$$\left(\frac{\partial T}{\partial e}\right)_\rho = \frac{(\gamma - 1)}{R} \quad \text{E.14}$$

$$\left(\frac{\partial T}{\partial \rho}\right)_e = \frac{1}{a}\left(\frac{\partial T}{\partial e}\right)_\rho \quad \text{E.15}$$

Using these relations, the speed of sound is calculated by using E.9.

Peng-Robinson Gas Thermophysical Model: This model actually modifies the SRK (Soave-Redlich-Kwong) equation of state in order to improve liquid density, vapor pressure and equilibrium ratio predictions. Peng-Robinson gas model is developed in 1976. The set of equations for this model is given as

$$\begin{cases} p(T,v) = \dfrac{RT}{v - b} - \dfrac{a\alpha^2(T)}{v^2 + 2bv - b^2} \\ e(T,v) = c_v T - \dfrac{a\alpha(T)(k+1)}{b\sqrt{2}}\tanh^{-1}\dfrac{b\sqrt{2}}{v + b} \\ s(T,v) = c_v \ln T + R\ln(v - b) - \dfrac{a\alpha(T)k}{b\sqrt{2TT_{cr}}}\tanh^{-1}\dfrac{b\sqrt{2}}{v + b} \end{cases} \quad \text{E. 16}$$

New set of parameters for Peng-Robinson model are $\alpha(T)$, a and b. $\alpha(T)$ is dependent on the temperature and it is a measure of intermolecular attraction force. Constants are a and b are both critical temperature and pressure dependent parameters. These values can be calculated via following set of equations.

$$\begin{cases} a = 0.45724\dfrac{(RT_{cr})^2}{p_{cr}} \\ b = 0.0778\dfrac{RT_{cr}}{p} \\ \alpha(T,\omega) = \left[1 + k\left(1 - \sqrt{\dfrac{T}{T_{cr}}}\right)\right] \\ k = \begin{cases} 0.37464 + 1.54226\omega - 0.26992\omega^2, & \omega \leq 0.49 \\ 0.379642 + 0.48503\omega - 0.164423\omega^2 + 0.016666\omega^3, & x > 0.49 \end{cases} \end{cases} \quad \text{E. 17}$$

where k is the thermal conductivity. As can be seen from above equations, $\alpha(T)$ is not only dependent on temperatue but also on acentric factor (ω) which is a function of the saturated vapor pressure and the critical pressure. This parameter also varies with the chemical composition of the gas. Entropy and energy equations are defined as the same as the ones in the perfect gas model for consistency.

Thermodynamic derivatives for Peng-Robinson gas model is a little bit challenging compared to both perfect gas and van der Waals thermopyhsical models. Peng-Robinson secondary properties are provided below:

$$\left(\frac{\partial p}{\partial e}\right)_\rho = \frac{\left(\frac{\partial p}{\partial T}\right)_\rho}{\left(\frac{\partial e}{\partial T}\right)_\rho} \quad \text{E. 18}$$

$$\left(\frac{\partial p}{\partial \rho}\right)_e = \left(\frac{\partial p}{\partial \rho}\right)_T - \left(\frac{\partial p}{\partial e}\right)_\rho \left(\frac{\partial e}{\partial \rho}\right)_T \quad \text{E. 19}$$

$$\left(\frac{\partial T}{\partial e}\right)_\rho = \frac{1}{\left(\frac{\partial e}{\partial T}\right)_\rho} \quad \text{E.20}$$

$$\left(\frac{\partial T}{\partial \rho}\right)_e = \left(\frac{\partial t}{\partial \rho}\right)_p - \left(\frac{\partial T}{\partial p}\right)_\rho \frac{\left(\frac{\partial e}{\partial T}\right)_p}{\left(\frac{\partial \rho}{\partial T}\right)_p} \quad \text{E. 21}$$

The complexity of second derivatives in the Peng-Robinson thermopysical model is due to the fact that the intermolecular attraction force is dependent on both temperature and acentric factor. Partial derivatives are implemented as follows:

$$\left(\frac{\partial p}{\partial T}\right)_\rho = \frac{R}{(v-b)} - \frac{2a\alpha'}{[v(v+b)+b(v-b)]} \qquad \text{E.22}$$

where

$$\alpha' = \frac{d\alpha}{dT} \qquad \text{E.23}$$

Other partial derivatives required for the secondary properties are given as follows:

$$\left(\frac{\partial e}{\partial T}\right)_\rho = \frac{R}{(\gamma-1)} - \frac{a}{b\sqrt{2}}\left[2\alpha\alpha' + k\alpha'\sqrt{\frac{T}{T_{cr}}} + \frac{1}{2}k\alpha(TT_{cr})^{-0.5}\right]f(v) \qquad \text{E.24}$$

$$\left(\frac{\partial p}{\partial \rho}\right)_T = -\frac{1}{\rho^2}\left(\frac{\partial p}{\partial v}\right)_T = -\left(-\frac{RT}{(v-b)^2} + \frac{2a\alpha'(v+b)}{[v(v+b)+b(v-b)^2]}\right)v^2 \qquad \text{E. 25}$$

$$\left(\frac{\partial e}{\partial \rho}\right)_T = -\frac{a\alpha(T)}{b\sqrt{2}}\left[\alpha(T) + k\sqrt{\frac{T}{T_{cr}}}\right]\frac{b\sqrt{2}}{a+2\rho b-\rho^2 b^2} \qquad \text{E. 26}$$

$$\left(\frac{\partial \rho}{\partial T}\right)_p = -\rho^2\left(\frac{\partial v}{\partial T}\right)_p \qquad \text{E.27}$$

$$\left(\frac{\partial T}{\partial \rho}\right)_p = \frac{1}{\left(\frac{\partial \rho}{\partial T}\right)_p} \qquad \text{E.28}$$

$$\left(\frac{\partial v}{\partial T}\right)_p = -\left(\frac{\partial p}{\partial v}\right)_T^{-1}\left(\frac{\partial p}{\partial T}\right)_v \qquad \text{E.29}$$

$$\left(\frac{\partial e}{\partial T}\right)_p = \left(\frac{\partial h}{\partial T}\right)_p - p\left(\frac{\partial v}{\partial T}\right)_p \qquad \text{E.30}$$

$$\left(\frac{\partial h}{\partial T}\right)_p = \left(\frac{\partial e}{\partial T}\right)_v + T\left(\frac{\partial p}{\partial T}\right)_v \left(\frac{\partial v}{\partial T}\right)_p \qquad \text{E.31}$$

As the final step, the speed of sound is computed by using E.9 and this finalizes the computation of Peng-Robinson gas model.

Experimental Test Setup

Cold gas thruster performance tests are conducted to observe the relationship between simulations and real conditions. The most important challenge for these tests was to simulate operational conditions which is the space environment. In order to obtain very low pressure levels close to vacuum, vacuum chamber test facility located in Roketsan is used. This facility is designed and manufactured completely by Turkish sub-contractors. Test facility has a cylindrical vacuum chamber of 3.1 m^3 with vacuum pumps as seen in Figure 9. Vacuum chamber can be depressurized down to 5 Pa. Sensors are required to track pressure and temperature inside the chamber real time.

Figure 9: Thrust chamber test setup

Test setup contains a propellant tank, a commercial regulator, a fill and drain system, a manifold, a thruster valve and the thruster itself with pressure and temperature sensors. Schematic drawing of the test setup is given in Figure 10. Pressure measurements are obtained at the propellant tank exit, regulator and manifold downstream, thruster valve upstream and thrust chamber. Temperature readings are taken from both tank exit and thrust chamber.

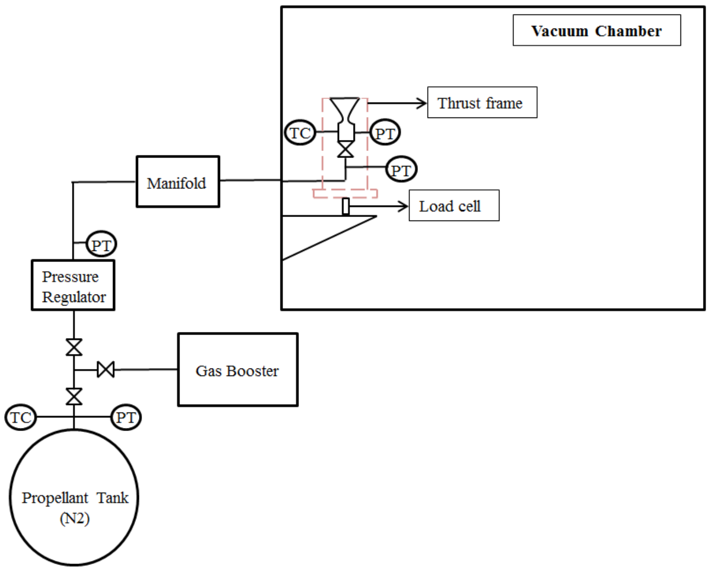

Figure 10: Test setup schematic drawing

Propellant tank is made from 4130 steel and painted to prevent corrosion. Propellant tank is pressurized by using a compressor booster. A 44-1362 series TESCOM regulator is used to lower the propellant pressure to operational pressure level. Thruster valve in the setup is also designed and manufactured by a Turkish company. It is a solenoid valve which operates at 28 V DC and with 1 A current. Pressure readings, except the one in the thrust chamber, are taken by using TRAFAQ EPI400.0A 8287 pressure transmitters. K-type thermocouples are used for temperature measurements. Kulite HKM-375 series pressure sensor is chosen to observe the pressure change inside the thrust chamber. Precision load cell of Burster 9431 series is used which has the capability to measure forces up to 500 N. Experimental test setup inside the vacuum chamber is given in Figure 11.

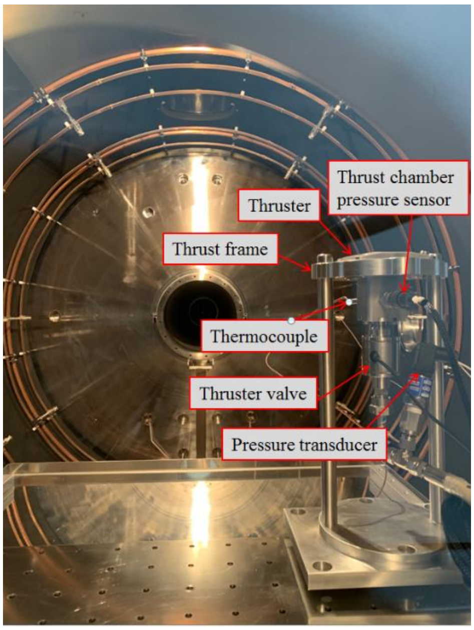

Figure 11: Thruster and thrust frame inside the vacuum chamber

Thrust frame, thruster and load cell are assembled in CAD program to ensure that the load cell and thrust are along the same axis. Pressure and temperature sensors are located inside the thrust chamber. Another pressure sensor is located prior to thruster valve. A flexible hose is used to accomplish feed through connection of the vacuum chamber.

RESULTS AND DISCUSSION

Application investigated in this study is a space application which involves very low pressure and temperature by its nature and it is necessary to determine whether the continuum postulate is valid at these conditions. The continuum approach is first validated to ensure that the Navier-Stokes equations are applicable.

Continuum Approach Validation

The Knudsen number, *Kn*, which is the ratio of the molecular mean free path of fluid to characteristic length, is used to determine whether the continuum postulate is valid or not [Greer, & Griep, 1967] and can be given by

$$Kn = \frac{Molecular\ mean\ free\ path}{Characteristic\ linear\ dimension\ of\ the\ flow\ field} \qquad \text{E.32}$$

For continuum Knudsen number is preferred to be close to zero as much as possible. However, if it is less than approximately 0.01, then continuum postulate is assumed to be applicable to the flow [Aksel, 2011].

Molecular mean free path (λ) is the distance traveled by a molecule between two consecutive collisions and can be obtained with following relation.

$$\lambda = \frac{k_B T}{\sqrt{2}\pi p d_m^2} \qquad \text{E.31}$$

Here k_B is the Boltzmann constant ($k_B = 1.38064910^{-23} J/K$), T is the gas temperature, p is the gas pressure and d_m is the molecular diameter of the gas.

Since lowest pressure and temperature are obtained at the exit section of the nozzle, this is the most critical section when continuum is considered. Exit pressure of the nozzle is 300 Pa and corresponding exit temperature is calculated as 28.9 K. Molecular diameter of nitrogen is found from literature as 3.64 Å [Kentish, Scholes, & Stevens, 2008]. Molecular mean free path is calculated as $2.2594x10^{-6}m$.

As mentioned above, since exit section is the critical section, exit diameter of the thruster is taken to be equal to the characteristic length. During the design of the thruster, exit diameter of the thruster is calculated as $25.7x10^{-3}m$. Finally, the Knudsen number is calculated and found as $8.79x10^{-5}$ which shows that the Knudsen number is still applicable for the analysis of the thruster in this study.

Verification of Thruster Nozzle

<u>Mesh Independency:</u> Mesh generation is very important in Computational Fluid Dynamics (CFD). Grid sizing is the key parameter for mesh generation and it is important for the accuracy and stability of numerical studies. The analyses in CFD are mesh dependent and optimum

mesh size and element number must be chosen in order to obtain correct solution within optimum computational time.

Six different mesh sizes are investigated and these meshes are given in Figure 12. Mesh generation is carried out by using unstructured NETGEN 1D-2D-3D algorithm in Salome.

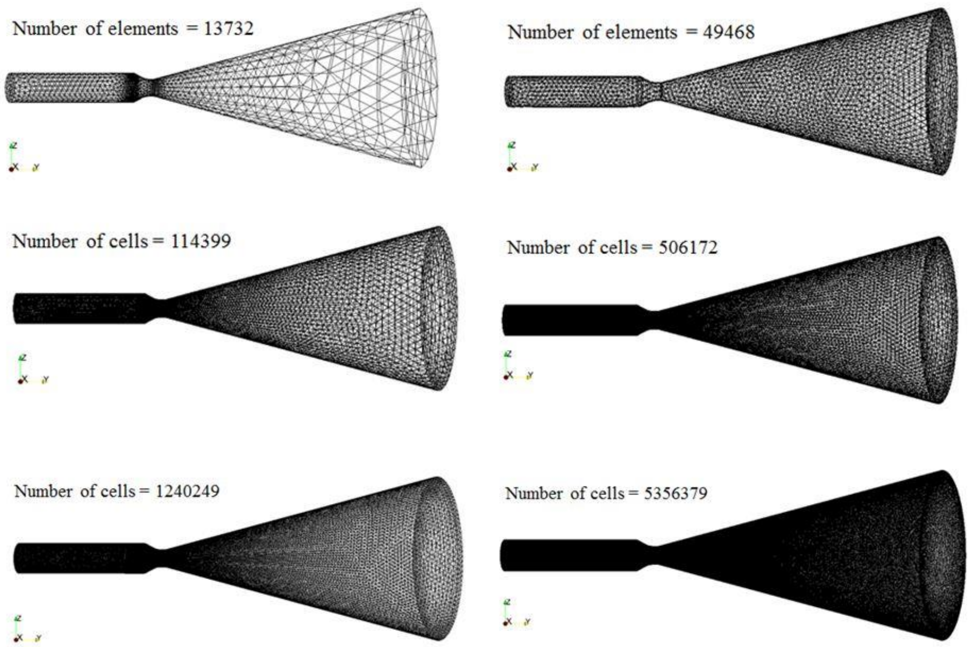

Figure 12: Different grids generated for mesh independency

Flow is simulated by using the Euler equations. Roe scheme is applied for the discretization of convective fluxes numerical method and ideal gas assumption is applied. Initial and boundary conditions are provided in Table 1. Pressure for initial condition is taken as 200 Pa since it is lower than the design nozzle exit pressure which is 300 Pa. Also it is foreseen that the vacuum chamber could achieve this pressure level after installation. Inlet boundary condition is defined as 10 bar and 293 K for the nominal operating conditions. Finally, to simulate vacuum condition, a pressure of 75 Pa is used at the exit section.

Table 1: Initial and boundary conditions for mesh independency studies

	Pressure (Pa)	Temperature (K)
Initial Condition	200	170
Boundary Conditions	$p_{inlet}=10^6$	$T_{inlet} = 293$
	$p_{outlet}=75$	

Analyses are carried out in terms of temperature, pressure, density and mass flow rate per area for throat values. Results (Table 2) show that all grids predict the location where maximum mass flow rate per cross section is occurred correctly.

Table 2: Comparison of mesh independency results

Mesh size	Temperature [K]	%Error in temperature	Pressure [bar]	%Error in pressure	Density [kg/m^3]	%Error in density	Mass flow rate per area [kg/m^{2}s]	%Error in mass flow rate per area
13732	240.43	1.53	5.01	5.11	7.01	4.10	2321.4	1.84
49468	241.59	1.05	5.03	4.70	6.97	4.65	2248.3	4.93
114399	241.49	1.09	5.08	3.79	7.09	3.01	2392.3	1.16
506172	239.24	2.02	4.92	6.82	6.93	5.20	2324.9	1.69
1240249	238.26	2.42	4.86	7.95	6.87	6.02	2319.9	1.90
5356379	235.78	3.43	4.68	11.36	6.68	8.62	2313.6	2.29

In terms of pressure, density and mass flow rate per area, grid size of 114399 shows closer results to theoretical ones. Grid size of 49468 gives the lowest error for temperature. However, values obtained for both grids are very close to each other. Hence, grid size of 114399 is chosen for the rest of the numerical analyses.

<u>Nominal Temperature Operating Conditions:</u> Nominal operating conditions are 10 bar of chamber pressure and 293 K of gas propellant temperature. These values are used for the nozzle design. Experimental test setup is arranged according to the nominal operation conditions.

Vacuum chamber performance test result is given in Figure 13. It is seen that after the actuation of thruster valve, thrust and chamber pressure started to increase together. In a short period of time, it is seen that chamber pressure reached the steady state value of approximately 10.5 bar. This chamber pressure is obtained due to imprecise adjustment of the pressure regulator. Since thrust chamber is exposed to vacuum conditions prior to actuation thruster valve, pressure at the beginning is very close to zero. Prior to actuation of thruster valve, the load cell measures approximately 35 N. This corresponds to the total weight of thrust frame, thruster, thruster valve and measurement sensors. After steady state thrust is obtained, load cell shows approximately 45 N. Thus, thruster provides 10 N of thrust at nominal operational conditions as predicted.

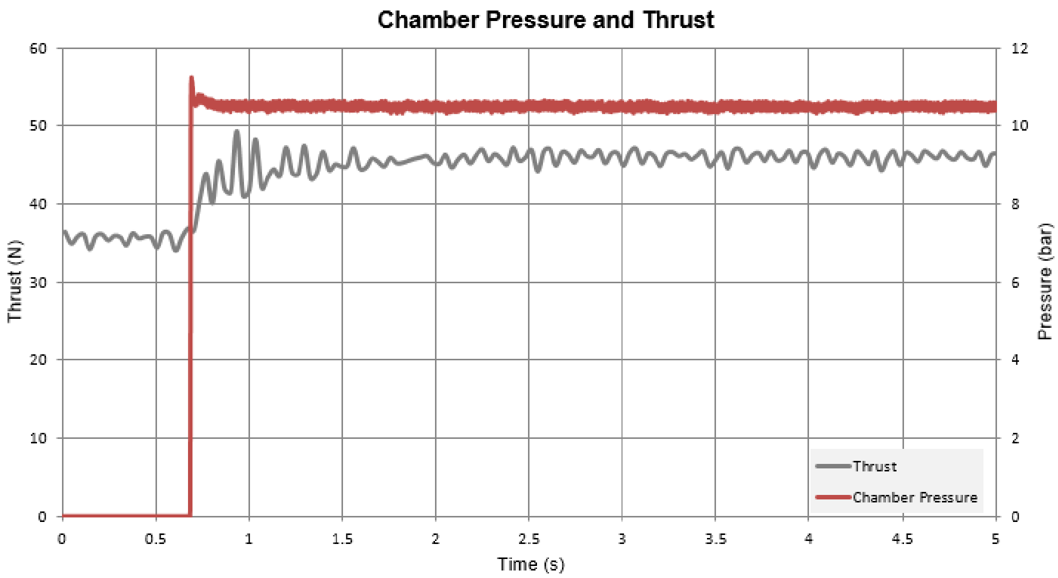

Figure 13: Nominal operating conditions vacuum chamber test results for chamber pressure (red line) and thrust (gray line)

Experimental values of the pressure and temperature in the thruster chamber which are 10 bar and 293 K, respectively, are used as the boundary conditions for the numerical analyses. Environmental pressure and temperature values, 200 Pa and 293 K are applied as the initial conditions.

Euler equations with Roe flux splitting scheme is used for the simulations. Steady state convergence is monitored when sufficient decrease in residuals is observed. For real gas models, Riemann boundary conditions are defined in SU^2 configuration file. CFL adaptation is used in between 0.4 and 5 to obtain faster convergence.

Numerical results of steady-state simulation of all gas models are provided in Figure 14. It is seen that ideal gas predicted lower chamber pressure than real gas models. Both real gas models predicted thrust chamber steady-state operation pressure closer to experimental values. Also since this thruster is designed to obtain 300 Pa at the exit section, it is also possible to state that the exit pressure obtained by real gas models are closer to the design exit pressure.

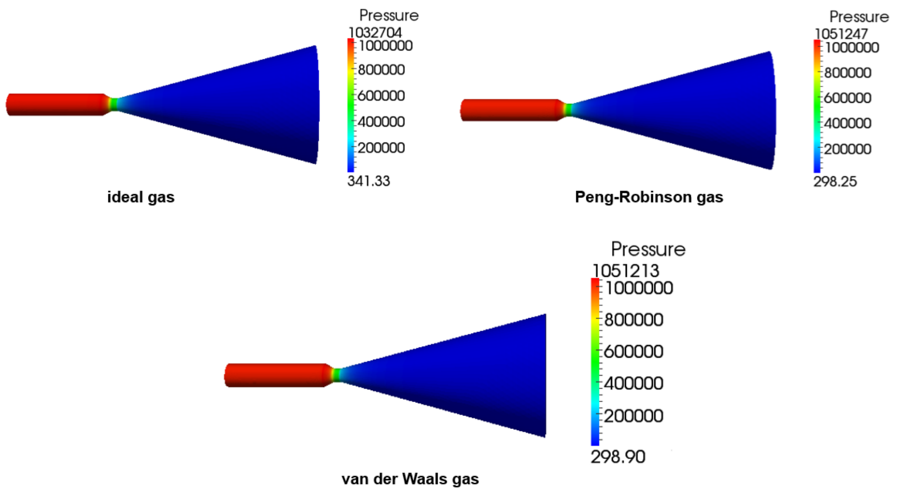

Figure 14: Nominal temperature operation condition results for different gas models

Thrust is calculated by area integration at the exit section of the nozzle by using open source flow visualization tool ParaView. Obtained thrust values are presented in Table 3. Real gas models obtained the same thrust, yet ideal gas model predicted a much higher thrust value. Even though the discrepancy between these models is not large, real gas models should be preferred.

Table 3: Thrust comparison between gas models

Gas Model	Thrust	% Error in Thrust
Ideal Gas	10.86	8.6
Peng-Robinson Gas	9.31	6.9
van der Waals Gas	9.31	6.9

Finally, computational time of these simulations should be considered. In preliminary design phase, it is necessary to obtain the results as fast as possible to predict performance parameters correctly. Ideal gas simulation takes approximately 600 minutes while Peng-Robinson gas model converged approximately in 170 minutes. Fastest solution is obtained in van der Waals gas model within 159 minutes. As a result, it seems appropriate to use van der Waals gas model for the analyses at nominal temperature operation condition.

<u>Low Temperature Operating Conditions:</u> Low temperature operating conditions are 10 bar of chamber pressure and 243 K of gas propellant temperature. In order to obtain 243 K of propellant temperature, firstly propellant tank is thermally conditioned to 262 K by using a

thermal chamber for 2.5 hours. Then, to obtain 243 K of propellant temperature, mass flow rate through the propellant tank is increased with the help of extra flexible hoses attached to the manifold. This method decreases the time to reach lower temperatures.

Vacuum chamber performance test result is given in Figure 15. Similar to nominal temperature results, after thruster valve actuation, thrust and chamber pressure starts to increase together. Steady-state chamber pressure value is obtained around 10 bar at the beginning but since propellant temperature continues to decrease, due to regulator's behavior, pressure inside the thrust chamber decreases. Before thruster valve actuation, load cell measures approximately 34 N. When the steady-state performance is obtained, the difference in the load cell measurements shows that approximately 10 N of thrust is obtained for low temperature operation conditions.

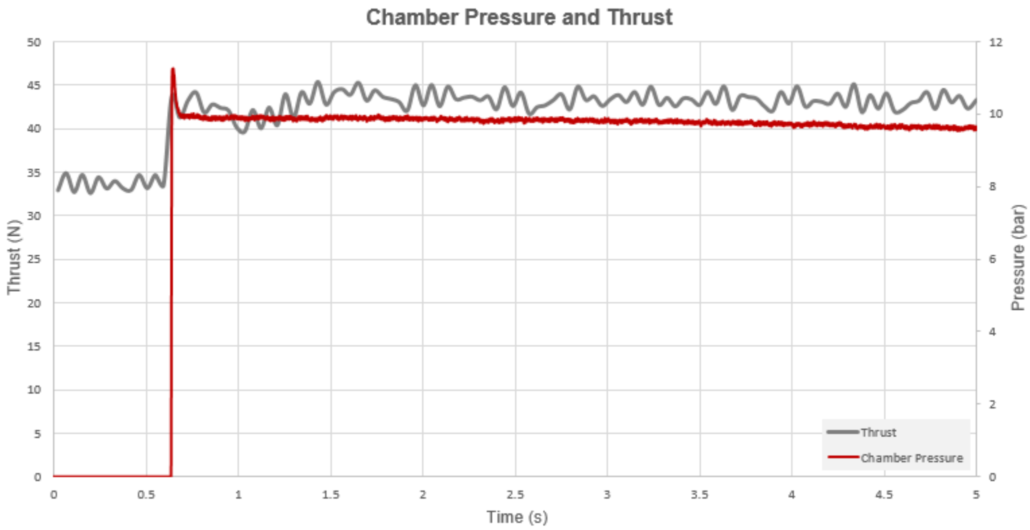

Figure 15: Low temperature operating conditions vacuum chamber test results for chamber pressure(red line) and thrust (gray line)

Experimental values of thruster chamber, 10 bar and 243 K are used as the boundary conditions for the numerical analyses. Environmental pressure and temperature values of 200 Pa and 293 K, respectively, are applied as initial conditions similar to the case with nominal temperature operating conditions.

Simulations have the same configuration as the nominal temperature operating conditions. Euler equations with Roe flux splitting scheme are used for the simulations. Riemann boundary condition is applied for real gas models. CFL adaptation is applied between minimum CFL of 0.4 and maximum CFL of 5.

As can be seen from Figure 16, again real gas models predicted closer thrust chamber pressure compared to ideal gas model. It is observed that the exit section temperatures are lower with respect to nominal temperature operating conditions. This is due to the lower chamber temperature and it is an expected result.

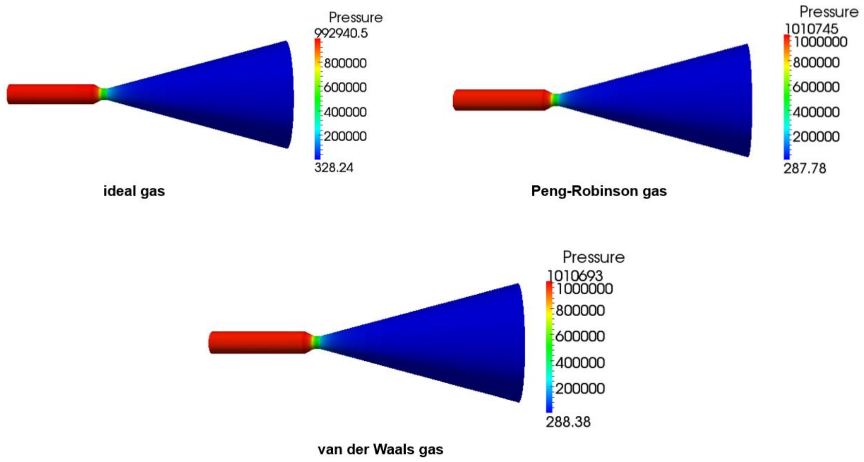

Figure 16: Low temperature operation condition results for different gas models

Thrust calculations are again performed by area integration at the thruster nozzle exit section and results are presented in Table 4. For low temperature operating conditions, ideal gas model seems to predict closer results to experimental values. However, for preliminary design phase, real gas models are also applicable by considering that they predict approximately 10% lower thrust than experimental values.

Table 4: Thrust comparison between gas models

Gas Model	Thrust	% Error in Thrust
Ideal Gas	10.44	4.6
Peng-Robinson Gas	9.01	9.9
van der Waals Gas	9.01	9.9

Lastly computational time of these simulations should be considered. Ideal gas simulation took 440 minutes, Peng-Robinson gas model took 162 minutes and van der Waals gas model are obtained within 152 minutes. Even though the thrust obtained is lower than experimental value, van der Waals gas model still the least time consuming model while predicting correct thrust chamber pressure.

Experimental and numerical studies showed that, van der Waals gas model is good enough to predict performance of a cold gas thruster for both nominal and low temperature operation conditions. Even though the obtained low temperature thrust value is lower than experimental values, general performance predictions are good enough for the preliminary design phase. Also, these performance predictions approximately takes 2 to 2.5 hours which is very favorable to compare many design alternatives during a very short time period.

For the future studies, effects of viscosity and turbulence can be investigated. Limits of propellant temperature can be forced and both experimental and numerical studies can be carried out. Also, real gas model implementations in SU^2 can be modified to improve the thrust predictions.

References

Aksel, M. H. (2011). *Fluid Mechanics*. Middle East Technical University.

Anis, A. (2012). *Cold Gas Propulsion System - An Ideal Choice for Remote Sensing Small Satellites.* Remote Sensing - Advanced Techniques and Platforms, IntechOpen.

Anis, A., (2008). *Design & Development of Cold Gas Propulsion System for Pakistan Remote Sensing Satellite (PRSS)*. 2nd International Conference on Advances in Space Technologies, pp. 49–53, IEEE.

Bzibziak, R. (2000). *Update of Cold Gas Propulsion at MOOG*. 36th AIAA/ASME/ SAE/ASEE Joint Propulsion Conference and Exhibit.

Gori, G., Guardone, A., Vitale, S., Head, A., Pini, M., & Colonna, P. (2015). *Non-Ideal Compressible-Fluid Dynamics Simulation with SU2: Numerical Assessment of Nozzle and Blade Flows for Organic Rankine Cycle Applications*. 3rd International Seminar on ORC Power Systems, Brussels, Belgium.

Greer, H., & Griep, D.J. (1967). *Dynamic Performance of Low-Thrust, Cold-Gas Reaction Jets in a Vacuum*. Journal of Spacecraft and Rockets, vol. 4, no. 8, pp. 983–990.

Hinkley, D. (2008). *A Novel Cold Gas Propulsion System for Nanosatellites and Picosatellites*. 22nd AIAA/USU Conference on Small Satellites, Logan, UT.

Jerman, T., & Langus, J. (2011). *Calculating Cold Gas Microthruster Velocity Flow Using Finite Volume Analysis*. University of Ljubljana, Ljubljana.

Kentish, S.E., Scholes, C.A., & Stevens, G.W. (2008). *Carbon Dioxide Separation Through Polymeric Membrane Systems for Flue Gas Applications*. Recent Patents on Chemical Engineering, vol. 1, no. 1, pp. 52–66.

Lemmer, K. (2017). *Propulsion for Cubesats*. Acta Astronautica, vol. 134, pp. 231– 245.

Manzoni, G., & Brama, Y. L. (2015). *Cubesat Micropropulsion Characterization in Low Earth Orbit*. 29th Annual AIAA/USU Conference on Small Satellites.

Matticari, G., Noci, G., Siciliano, P., Miccolis, M. & Strada, S. (2010). *Cold Gas Thruster Assembly for SGEO Platform: Review of Development Activities by Thales Alenia Space Italia*. Space Propulsion Conference, San Sebastian, Spain.

Lev,R., Herscovitz, J., & Zuckerman, Z. (2014). *Cold Gas Propulsion System Conceptual Design for the SAMSON Nano-satellite*. 50th AIAA/ASME/SAE/ASEE Joint Propulsion Conference, p. 3759.

Pini, M., Vitale, S., Colonna, P., Gori, G., Guardone, A., Economon, T., Alonso, J., & Palacios, F. (2017). *SU2: The Open-Source Software for Non-Ideal Compressible Flows*. Journal of Physics: Conference Series, vol. 821, p. 012013, IOP Publishing.

Ranjan, R., Chou, S., Riaz, F., & Karthikeyan, K. (2017). *Cold Gas Micro Propulsion Development for Satellite Application*. Energy Procedia, vol. 143, pp. 754–761.

Rickmers, P. (2004). *Performance Enhancement Through Flow Control in Cold Gas Thruster Nozzles*. 55th International Astronautical Congress.

Risi, B. W. (2014). *Propulsion System Development for the CanX-4 and CanX-5 Dual Nanosatellite Formation Flying Mission*. University of Toronto.

Sarda, K., Grant, C., Eagleson, S. Kekez, D., & Zee,R. (2008). *Canadian Advanced Nanospace Experiment 2: On-orbit Experiences with a Three-kilogram Satellite*. 22nd AIAA/USU Conference on Small Satellite, Logan, UT.

Shephered, D. (1972). *Aerospace Propulsion*. Elsevier Science Ltd.

Zandbergen, B. (2000). *Modern Liquid Propellant Engines, 2000 Outlook*. Delft University of Technology, Faculty of Aerospace Engineering, The Netherlands.